JACS
JOURNAL OF THE AMERICAN CHEMICAL SOCIETY
Article
pubs.acs.org/JACS

# Effect of Internal Cavities on Folding Rates and Routes Revealed by Real-Time Pressure-Jump NMR Spectroscopy

Julien Roche,[†,∥] Mariano Dellarole,[†,∥] José A. Caro,[‡] Douglas R. Norberto,[§] Angel E. Garcia,[⊥] Bertrand Garcia-Moreno,[‡] Christian Roumestand,[†] and Catherine A. Royer*[,†,#]

[†]Centre de Biochimie Structurale, INSERM U554, CNRS UMR 5048, Universités de Montpellier, France

[‡]Department of Biophysics, Johns Hopkins University, Baltimore, Maryland 21218, United States

[§]Department of Biochemistry, Institute of Biology, University of Campinas, Campinas, Brazil

[⊥]Department of Physics and Applied Physics and Center for Biotechnology and Interdisciplinary Studies, Rensselaer Polytechnic Institute, Troy, New York 12180, United States

Supporting Information

**ABSTRACT:** The time required to fold proteins usually increases significantly under conditions of high pressure. Taking advantage of this general property of proteins, we combined P-jump experiments with NMR spectroscopy to examine in detail the folding reaction of staphylococcal nuclease (SNase) and of some of its cavity-containing variants. The nearly 100 observables that could be measured simultaneously collectively describe the kinetics of folding as a function of pressure and denaturant concentration with exquisite site-specific resolution. SNase variants with cavities in the central core of the protein exhibit a highly heterogeneous transition-state ensemble (TSE) with a smaller solvent-excluded void volume than the TSE of the parent SNase. This heterogeneous TSE experiences Hammond behavior, becoming more native-like (higher molar volume) with increasing denaturant concentration. In contrast, the TSE of the L125A variant, which has a cavity at the secondary core, is only slightly different from that of the parent SNase. Because pressure acts mainly to eliminate solvent-excluded voids, which are heterogeneously distributed throughout structures, it perturbs the protein more selectively than chemical denaturants, thereby facilitating the characterization of intermediates and the consequences of packing on folding mechanisms. Besides demonstrating how internal cavities can affect the routes and rates of folding of a protein, this study illustrates how the combination of P-jump and NMR spectroscopy can yield detailed mechanistic insight into protein folding reactions with exquisite site-specific temporal information.

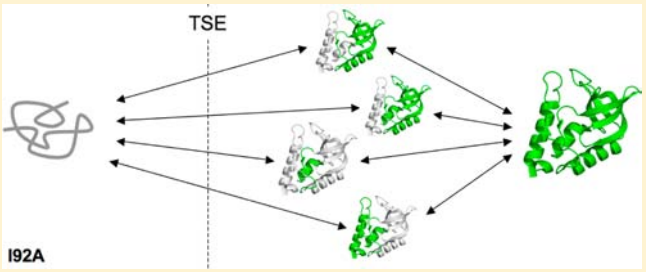


## INTRODUCTION

The complete description of a protein folding reaction requires detailed understanding of how the environment of every atom of each individual protein molecule in the ensemble in solution evolves during the reaction. In practice, this is far beyond what can be achieved with the majority of protein folding studies. Most of these studies depend on global physical and spectroscopic observables such as fluorescence, circular dichroism, FTIR, or SAXS, which provide ensemble averages and do not offer anything close to the desired spatial or temporal resolution. Some techniques such as Förster resonance energy transfer (FRET) have the temporal resolution and single-molecule sensitivity requisite to describe the underlying heterogeneity of the ensemble[1] but lack high spatial resolution. Increasing spatial resolution has been addressed by the recent introduction of IR probes in the backbone and side chains at specific positions of a protein, coupled with ultrafast T-jump IR spectroscopy. These experiments have allowed differentiation of the time scales of backbone and side chain ordering.[2] The problem with this approach, as with FRET, is that the acquisition of site-specific information at multiple residues of the chain requires the separate preparation of protein variants modified at each residue (or pair of residues) of interest and a separate set of experiments for each. It is clear that much remains to be understood about the detailed, physical character of the protein folding reaction. Here we show that pressure, coupled with NMR spectroscopy and mutagenic analysis, can be used to examine details of the protein folding reaction that have been experimentally inaccessible until now.

Multidimensional NMR spectroscopy is one of the experimental techniques with the potential to contribute a high-resolution, site-specific, time-resolved description of the protein folding reaction. In the rare cases of ultraslow folding proteins, classical multidimensional real-time NMR has been quite useful.[3−10] Site-specific monitoring of the folding process can be achieved with quench-flow H/D exchange, but detection is not performed in real time (separate samples are required for

Received: April 16, 2013
Published: August 30, 2013

   dx.doi.org/10.1021/ja406682e | J. Am. Chem. Soc. 2013, 135, 14610−14618

each time point).[11,12] Relaxation dispersion techniques probe dynamic exchange on the microsecond to millisecond time scale, relevant for the study of protein folding, but their application to the study of the protein folding reaction proper has been limited.[13,14] More generalized real-time unfolding of proteins by T-jump or rapid mixing experiments has been limited to 1D NMR experiments with a small number of signals, such as high-field-shifted methyl protons, $^{19}$F or specific-labeled tryptophan.[15−25] Recent advances in multidimensional NMR acquisition have extended the accessible time scale down to the order of seconds,[26−28] providing access to faster folding systems. These advances in NMR approaches can be coupled with methodology for pressure-jump NMR experiments to enable a new type of studies of the protein folding reaction with site-specific resolution. Pressure-induced unfolding of proteins is uniquely useful for these studies because the molar volume of the transition-state ensemble (TSE)[29−38] is larger than that of the unfolded state. For this reason, the activation volume for folding of proteins is positive, and as a result, the folding reactions that occur in seconds or less at atmospheric pressure can be slowed to minutes and even hours at high pressure. Thus, high pressure can be used to slow protein folding reactions and to make them compatible with the time scale of multidimensional NMR spectroscopy.

We have performed P-jump studies monitored with Trp fluorescence and real-time $^{1}$H−$^{15}$N HSQC relaxation on staphylococcal nuclease (SNase), its hyperstable variant Δ+PHS SNase, as well as on variants of this hyperstable construct that have internal cavities,[39] the result of substitution of internal positions with Ala (Figure 1). The volume difference

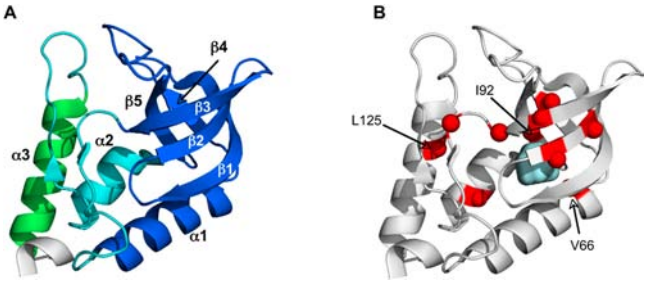


**Figure 1.** (A) Structure of Δ+PHS with the secondary elements labeled (α1−3, helix; β1−5, strand).[49] The subdomain organization in Δ+PHS is indicated as follows: SubD1 consisting of the first 96 residues that form a five-stranded β-barrel (β1−β5) and an abutting α-helix (α1) (blue), IntD (cyan) (α-helix 2, residues 99−105 and residues 39−40 and 110−111), and SubD2 (α-helix 3), spanning residues 122−134 (green). (B) Structure of Δ+PHS (3BDC) with the Cα position of the 10 alanine substitutions indicated with red spheres. The naturally occurring cavity in the Δ+PHS structure is drawn in cyan. The shape and size of this cavity were calculated with the McVol algorithm[54] using a 0.12 nm probe.

between the folded and unfolded forms of these variants is larger than for the true WT SNase and for the highly stable Δ+PHS variant.[39,40] The activation volumes accompanying folding of the cavity variants revealed the extent to which solvent-excluding voids are already formed at the folding barrier. In variants in which the cavities are present in the central and main core of the protein (denoted SubD1), the structural ensemble at the folding barrier was much more open and structurally heterogeneous, lacking much of the solvent-excluding void volume of the TSE of the wild-type. In contrast, the TSE of a variant in which the cavity was engineered in a secondary core, located between the C-terminal subdomain 2 (SubD2) and the interface domain (IntD), had properties comparable to the WT, characterized by a disordered SubD2 and an ordered central core (SubD1).[29−31] In variants with the cavity deep in the hydrophobic core of SubD1, the open TSE observed at low denaturant concentration became volumetrically more like that of the native state as denaturant concentration was increased. The site-specific, kinetic heterogeneity revealed by these experiments suggests that introduction of cavities in the main core of SNase can change a single-pathway folding reaction into one with multiple and structurally distinct folding routes and that the fluxes across the different routes can be modulated by denaturant.

## RESULTS

**Fluorescence-Detected Pressure-Jump Experiments.** Trp-140 fluorescence-detected pressure-jump (P-jump) relaxation profiles of the folding/unfolding of Δ+PHS SNase, WT SNase, and 10 cavity-containing variants in the Δ+PHS reference protein (Figure 2 and Supporting Information Figure

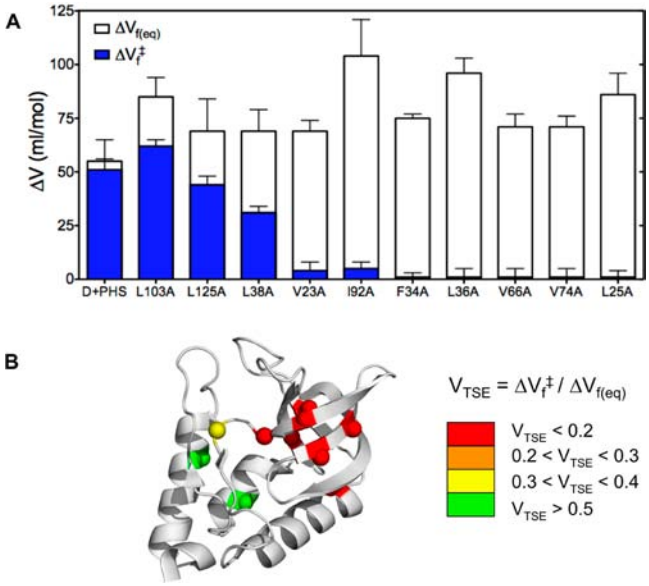


**Figure 2.** (A) Comparison of the equilibrium volume change for folding ($\Delta V_f^{\circ}$) (reproduced from ref 40) and the activation volume for folding ($\Delta V_f^{\ddagger}$) measured in the present study from fluorescence-detected P-jump kinetics, for Δ+PHS and the 10 cavity-containing variants of Δ+PHS. (B) Ten cavity-creating variants of Δ+PHS residues are colored on the structure according to the extent to which mutation to alanine leads to large decreases in the relative volumes of the TSE: $V_{TSE} = \Delta V_f^{\ddagger}/\Delta V_f^{\circ}$ measured from fluorescence experiments. Red corresponds to very small $V_{TSE}$ values, while green corresponds to relatively high $V_{TSE}$ values.

S1) exhibited single-exponential kinetics.[29] The Δ+PHS reference protein bears three stabilizing mutations in the C-terminal helix (P117G, H124L, and S128A), and the flexible loop 44−51 is replaced by F50 and N51. The simplicity of the folding/unfolding reactions at high pressure has been observed previously for WT SNase and arises from the pressure-induced slowing of the reaction, eliminating the contribution of proline isomerization.[41] Unlike WT SNase, the high stability of Δ+PHS and its cavity variants required addition of guanidinium hydrochloride (GuHCl) to observe unfolding in the pressure


dx.doi.org/10.1021/ja406682e | J. Am. Chem. Soc. 2013, 135, 14610−14618

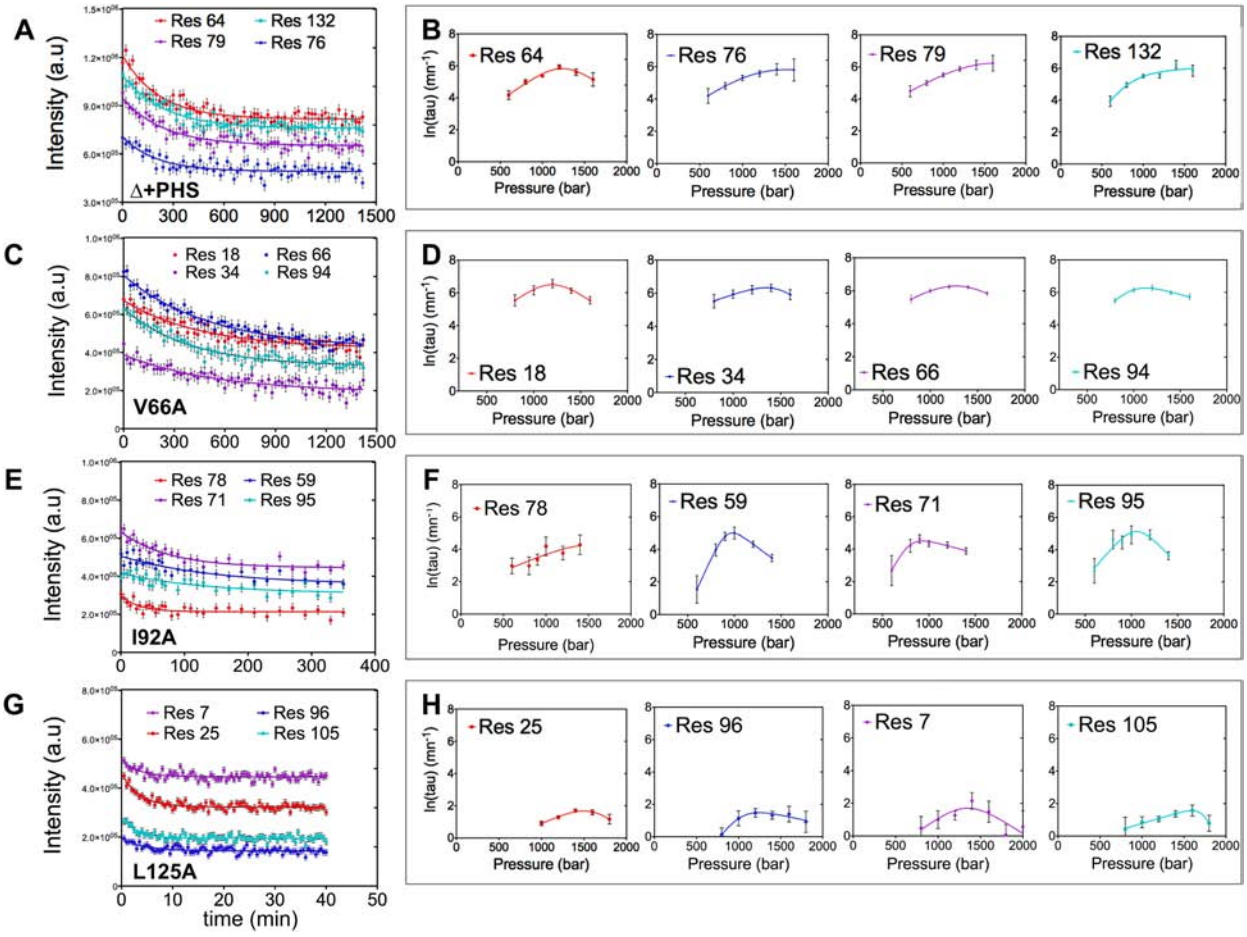


**Figure 3.** P-jump kinetics monitored by real-time NMR. Examples of the intensity decay of $^{15}N-^{1}H$ amide cross-peaks for four representative residues are shown for (A) Δ+PHS ($p$ = 1000 bar, [GuHCl] = 2 M); (C) V66A ($p$ = 1200 bar, [GuHCl] = 1.1 M); (E) I92A ($p$ = 1000 bar, [GuHCl] = 0.85 M); and (G) L125A ($p$ = 1200 bar, [GuHCl] = 0.85 M). The intensity decay was monitored by recording the time series of $^{15}N-^{1}H$ HSQC spectra (Δ+PHS and V66A) or $^{15}N-^{1}H$ SOFAST-HMQC (I92A and L125A). The corresponding fits of the pressure dependence of the relaxation time $\tau$ are displayed in the right panels, for (B) Δ+PHS, (D) V66A, (F) I92A, (H) L125A.

range accessible with the instrument used (<3 kbar). The pressure dependence of the natural logarithm of the P-jump relaxation time, ln $\tau$ (Figure S2), was analyzed for each variant according to a two-state folding/unfolding relaxation model (see Materials and Methods section). As described previously,[30,31] the values for the rate constant and activation volume for either folding or unfolding ($k_f^o$ or $k_u^o$ and $\Delta V_f^{\ddagger}$ or $\Delta V_u^{\ddagger}$) were constrained by the equilibrium volume changes ($\Delta V_f^o$) and free energies ($\Delta G_f^o$) for folding obtained previously under these conditions.[39,40] The ratio, $V_{TSE} = \Delta V_f^{\ddagger}/\Delta V_f^o$, represents the volumetric position of the TSE, with respect to the total difference in volume between the folded and unfolded states. The $V_{TSE}$ value is the equivalent of the $m_f^{\ddagger}/m_{eq}$ value commonly used to define the degree of exposed surface area in the TSE and here measures the response of the protein folding kinetics to pressure.[31]

For Δ+PHS and WT SNase, the significant pressure-dependent increases in the folding relaxation times (Figures 2 and S2), indicative of large positive activation volumes for folding, and near zero activation volume for unfolding leads to a $V_{TSE}$ value near unity, indicative of a TSE that is volumetrically very native-like,[29−31] as observed previously for WT SNase.[29] In contrast, the seven variants (V23A, I92A, F34A, L36A, V66A, V74A, and L25A—all in the Δ+PHS background) containing cavities within SubD1 exhibited a large and negative activation volume for unfolding $\Delta V_u^*$ (Figures 2 and S2), revealing a TSE that was volumetrically close to the unfolded state. The L38A, L103A, and L125A variants with cavities in the interface between domains showed intermediate behavior, with TSEs between the folded and unfolded states in terms of molar volume (Figure 2).

**Real-Time Pressure-Jump NMR Spectroscopy.** The previous NMR-detected equilibrium pressure unfolding study on the SNase cavity variants[39,40] revealed significant and distinct folding intermediates. To probe further the structural heterogeneity of these folding reactions, real-time P-jump two-dimensional NMR relaxation experiments were performed with the true WT SNase and four of the Δ+PHS variants: (1) the reference Δ+PHS protein; (2) the L125A variant, bearing a cavity at the interface between SubD2 and the IntD; and (3,4) the I92A and V66A variants with an enlarged cavity in the central OB-fold of SubD1. Between 20 and 80 $^{1}H-^{15}N$ HSQC-like spectra were collected for these variants as a function of time after small pressure jumps (Figure S3). Multiple GuHCl concentrations were tested to explore the effect of denaturant itself on the volumetric properties and heterogeneity of these proteins. The time dependence of over 15 000 individual cross-peak intensities from all detectable amide groups for these five proteins was well-described by single-exponential relaxation times ($\tau$) (Figure 3A,C,E,G and Figures S4 and S5). However,


dx.doi.org/10.1021/ja406682e | J. Am. Chem. Soc. 2013, 135, 14610−14618

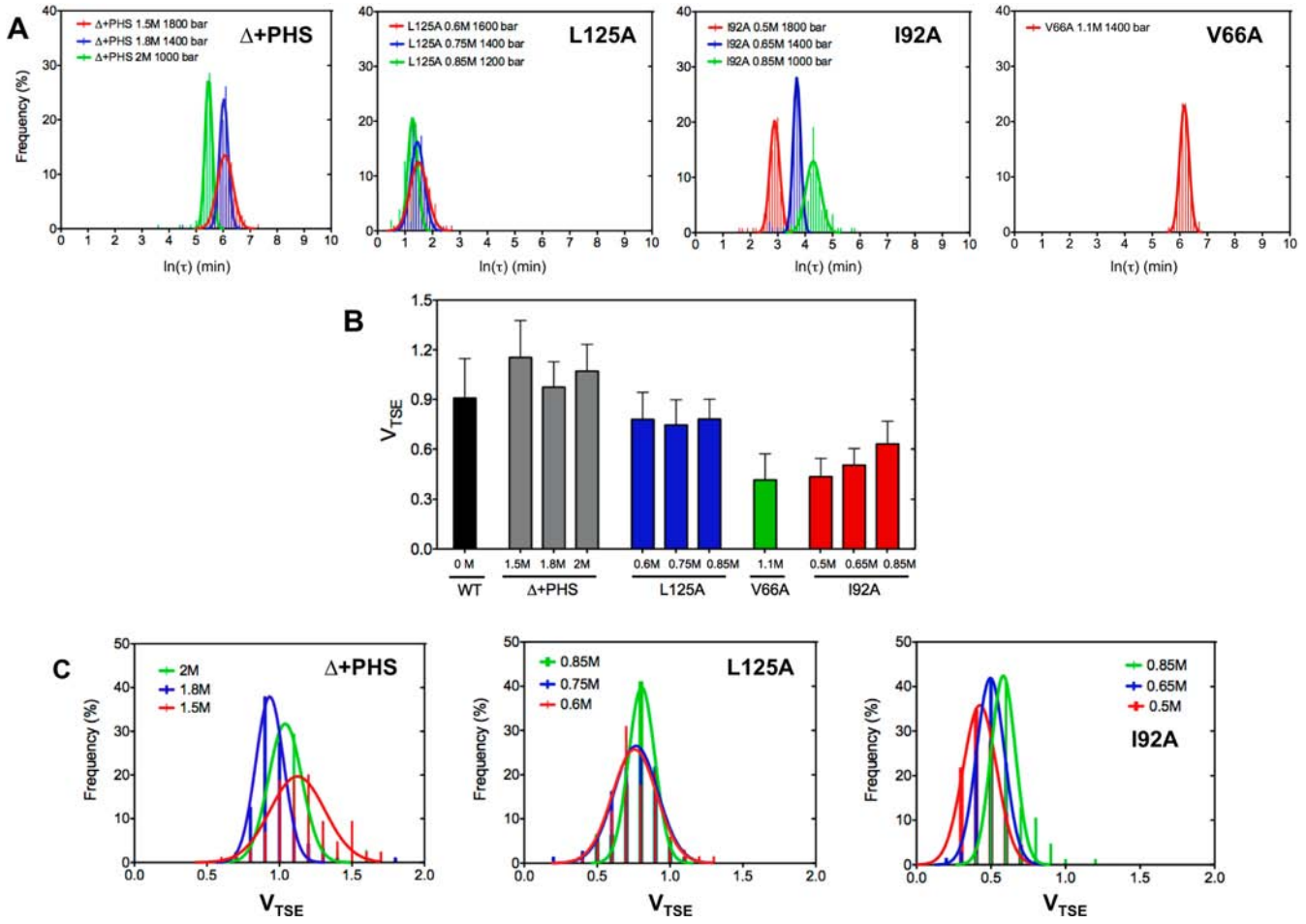


**Figure 4.** Kinetic heterogeneity from P-jump NMR (A) ln $\tau$ distributions for Δ+PHS and the cavity-containing variants at the pressure unfolding midpoints for each condition as labeled. (B) Averaged relative volume of the TSE, $V_{TSE} = \Delta V_f^{\ddagger}/\Delta V_f^{o}$, measured by NMR-detected P-jump kinetics, is shown for the WT SNase, Δ+PHS, L125A, I92A, and V66A at the different concentrations of GuHCl tested. For each protein, the $V_{TSE}$ values were averaged over all measurable amide groups. The error bar represents the standard deviation of the $V_{TSE}$ value distribution. (C) $V_{TSE}$ distributions for Δ+PHS (left), L125A (center), and I92A (right) at the indicated GuHCl concentrations of the residue-specific values obtained from analysis of the pressure-jump NMR relaxation profiles.

the values of $\tau$ for the different residues of each variant differed significantly among themselves, in particular, in the case of the I92A variant (Figure S5). The ln $\tau$ values near the pressure unfolding midpoint, $p_{1/2}$ (where the dynamic range was maximal and experimental uncertainty minimal), were rather broadly distributed for all variants (Figure 4A and Figures S6–8), revealing significant kinetic complexity. Interestingly, for the I92A variant, the kinetic heterogeneity first decreased and then increased again with increasing denaturant. Under conditions of similar stability, the different SNase variants exhibited very different time scales for relaxation.

The pressure dependence of each ln $\tau$ versus pressure plot (Figure 3B,D,F,H and Figure S4) was analyzed to yield residue-specific $V_{TSE}$ distributions (Figures 4B,C and S9). The average $V_{TSE}$ values for WT SNase and Δ+PHS were near unity, within experimental uncertainty, despite the fact that the overall equilibrium $\Delta V_f^{o}$ increased with GuHCl.[39] The $V_{TSE}$ value for L125A, with an extra cavity between SubD2 and the IntD, was found to be near 0.8 on average and also independent of denaturant concentration. In contrast, the I92A and V66A variants, with enlarged cavities in the central OB-fold in SubD1, exhibited much lower $V_{TSE}$ values, near 0.4, due to a large and negative $\Delta V_u^{\ddagger}$. Moreover, the $V_{TSE}$ for I92A showed interesting Hammond-like behavior, becoming larger (more native-like in volume) with increasing denaturant. The $V_{TSE}$ values obtained from NMR for the V66A and I92A cavity-containing variants, while smaller than for WT and Δ+PHS, are not as low as those obtained from fluorescence. The ln $\tau$ versus pressure profiles for the I92A variant obtained by fluorescence and the Trp-140 NH amide resonance intensity at similar GuHCl concentration are very similar (Figure S10). Hence, the observed differences between the $V_{TSE}$ values obtained from fluorescence and those obtained from the average of the $V_{TSE}$ value distribution from NMR arise from residue-specific rather than technique-specific effects.

**Structural Mapping of Kinetic Complexity.** Structural mapping of the heterogeneity of the kinetic pressure effect ($V_{TSE}$) revealed that most of the large $V_{TSE}$ values for Δ+PHS are found in helix 2 and in the $\beta$-barrel, the most stable region of the protein and the one that surrounds the central cavity (highlighted by the ovoid in Figure 5, top left). In contrast, for the I92A variant, most of the large $V_{TSE}$ values (which are smaller in general than for the reference protein) are found in helix 3 (SubD2) at low denaturant concentration (ovoid in Figure 5, bottom left), and they shift toward SubD1 and then the IntD with increasing denaturant concentration. This


dx.doi.org/10.1021/ja406682e | J. Am. Chem. Soc. 2013, 135, 14610–14618

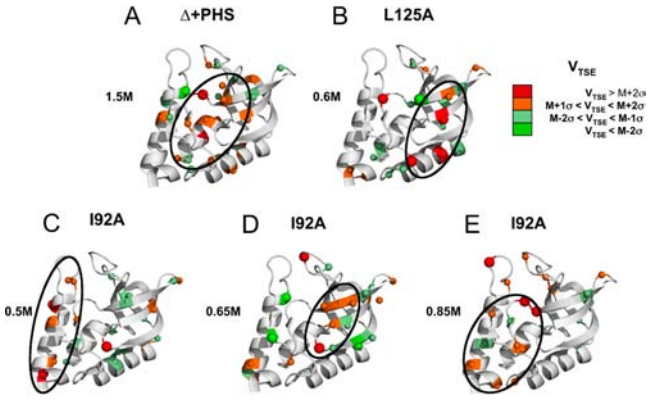


**Figure 5.** Structural mapping of the heterogeneity of the $V_{TSE}$ of Δ+PHS, L125A, and I92A. Residues with strongly deviating $V_{TSE}$ values are color coded on the structure as shown. (A) Δ+PHS, which is characterized by high $V_{TSE}$ values in SubD1 (note the high $V_{TSE}$ values inside the ovoid). (B) L125A, the large $V_{TSE}$ values are shifted to the N-terminal side of the OB-fold (SubD1). (Note the high $V_{TSE}$ values inside the ovoid). (C−E) TSE of I92A presents large $V_{TSE}$ values in the C-terminal helix at low denaturant that shift to the N-terminal region of the OB-fold and then to the core of the protein and IntD with increasing denaturant concentration. (Note the high $V_{TSE}$ values inside the ovoid). The structural shift in the $V_{TSE}$ values is correlated with the Hammond effect measured for this variant.

structural shift of the pressure effect with increasing denaturant concentration occurs concomitantly with an overall increase in the $V_{TSE}$ values and with a narrowing followed by an increase in the width of the distribution of ln $\tau$ values. Structural mapping of ln $\tau$ (Figures S11−13) is consistent with the $V_{TSE}$ mapping.

## DISCUSSION

**$V_{TSE}$ and Cavity Formation in the TSE.** Our previous equilibrium pressure unfolding studies of these SNase variants demonstrated that the introduction of internal cavities significantly increased the difference in molar volume between their folded and unfolded states.[39] Hence, the existence of internal solvent-excluded void volume in the folded states of proteins that is eliminated upon unfolding represents a major contributing factor to the effect of pressure on protein stability. We have also shown previously[37] that the value of the volume change upon unfolding (the magnitude of the pressure effect), unlike the denaturant $m$ value, does not depend upon the amount of exposed surface area in the unfolded state. We concluded from this that density differences in the solvent upon hydration of exposed surface area, compared to the bulk, were not an important factor governing the value of the volume change of unfolding. As previously observed, as well,[42] the effect of pressure on the folded-state HSQC resonances of these variants was more pronounced for the I92A variant with the cavity in the central core than for the L125A variant with the cavity in SubD2, consistent with the existence of excited states in the folded-state basin of the I92A variant. In contrast, the L125A variant exhibited more profound differences in chemical shift at atmospheric pressure with respect to the reference Δ+PHS, consistent with structural adjustment of the folded state to the mutation, whereas those observed for the I92A variant were minimal.

The present P-jump kinetics studies provide a volumetric characterization of the structural ensembles of these SNase variants at the folding barrier. The molar volumes of the WT SNase and Δ+PHS TSE's are very close to that of the folded state. Introduction of cavities in the C-terminal SubD2 or in the IntD does not perturb the folding pathway significantly, and the TSEs remain native-like for these variants. In contrast, the introduction of cavities in the central OB-fold core of the protein drastically decreased the molar volume of the TSE relative to the folded state. The destabilization of SubD1, by alanine substitution (I92A or V66A) or introduction of ionizable residues,[31] leads to considerable destabilization of the reference TSE. In this case, the folding pathway is modified, and the structural ensemble of the protein at the barrier is much different, with core cavities much more hydrated than is normally the case. Like the volumetric Hammond behavior observed previously for tendamistat,[33,43] the structural ensemble at the barrier becomes more native-like for the I92A variant as denaturant concentration is increased. Apparently, the most open configurations are preferentially stabilized by the denaturant and contribute increasingly less to the folding barrier. In contrast, introducing cavities at the interface between SubD1 and SubD2 (L125A and L103A substitutions), while also increasing the change in molar volume of upon unfolding,[31] also leads to intermediate effects on the volume of the TSE relative to the folded and unfolded states. We observed previously position-dependent effects on the $V_{TSE}$ upon substitution of buried leucine or valine residues by lysine.[31] Introduction of lysine at position 125 had no effect on the $V_{TSE}$. On the basis of this observation, we proposed that the TSE of both the WT SNase and the Δ+PHS protein exhibits a collapsed SubD1 from which solvent has already been excluded and cavities formed, but with significant disorder in SubD2 and the IntD. The present results with cavity-containing variants are consistent with this interpretation. Introduction of a cavity near position 125 does not modify the TSE, which retains a solvent-excluded SubD1 and a disrupted SubD2. Such a TSE would be expected to present cavities in the former but not at the interface, hence presenting a lower fractional volume at the barrier than the reference protein.

**Effect of Cavities on Folding/Unfolding Rates.** The P-jump relaxation times of the four proteins (SNase WT, Δ+PHS, I92A, and L125A) at $p_{1/2}$ differ by over 2 orders of magnitude. Some of these differences reflect differences in denaturant concentration or pressure at $p_{1/2}$. However, perturbations of the energy levels of the different states on the folding landscape by the mutations must contribute, as well. The I92A and L125A variants have similar stability; under similar conditions, they showed a 20-fold difference in relaxation times that must originate with a difference in the barrier heights for folding and/or unfolding. A higher energy barrier to folding for the I92A variant compared to the L125A variant is entirely consistent with our hypothesis that the TSE for the L125A variant is equivalent to that of the WT SNase and reference Δ+PHS protein, with a collapsed SubD1 from which solvent has already been excluded, and a disrupted SubD2, whereas for the 192A variant, the TSE involves a higher energy heterogeneous ensemble that is partially unfolded in SubD1, as well. The 20-fold difference between the relaxation times of WT SNase and Δ+PHS can be accounted for by the much higher thermodynamic stability of Δ+PHS. This slows unfolding significantly and in addition forces use of 2 M GuHCl in the P-unfolding experiments, which slows folding further. The 50-fold difference in the relaxation time at the similar $p_{1/2}$ values for Δ+PHS and the L125A variant can be explained by a combination of higher concentration of denaturant needed in


dx.doi.org/10.1021/ja406682e | J. Am. Chem. Soc. 2013, 135, 14610−14618

the experiments with Δ+PHS, which slows its folding, and destabilization of the folded state of L125A by the mutation, which speeds up its unfolding.

**Structural Basis for Kinetic Heterogeneity.** The P-jump NMR spectroscopy experiments revealed significant heterogeneity, well beyond experimental uncertainty, in the relaxation times and $V_{TSE}$ values reported by individual residues. The large number of observables obtained with the P-jump 2D NMR clearly revealed the limits of the two-state approximation. While all of the profiles conformed to the single-exponential function expected for the two-state approximation, there was a large spread in their values reflecting the underlying complexity and structural heterogeneity of the folding reactions. Because of the very small free-energy differences between the multiples states revealed by the distributed apparent rates and volume changes, analysis in terms of multiple specific pathways is unfeasible. Nonetheless, it is of interest to consider whether the basis for the heterogeneity in barrier heights arises from the population of intermediates with distinct free energies on the folded side of the barrier (hence leading to heterogeneity in the unfolding rates) or whether there is structural and energetic heterogeneity at the folding barrier, itself. High-pressure NMR spectroscopy studies on the WT and Δ+PHS SNase and the Δ+PHS/L125A variant showed previously that an intermediate with a folded SubD1 and a disordered SubD2 is populated not only transiently[44,45] but also under certain equilibrium conditions.[40] This intermediate is similar to the ensemble at the TSE for the reference protein and is a major feature of the SNase free-energy landscape. We propose that for Δ+PHS and WT SNase, the kinetic heterogeneity arises from the population of this intermediate ensemble in the ground state. In the TSE, the tertiary interactions in SubD1, which are nearly fully in place in this intermediate, are not yet present (Figure 6).

On the basis of the $V_{TSE}$ value for the L125A variant and previous equilibrium studies that revealed unfolding intermediates involving both the C-terminus, similar to Δ+PHS, but also the N-terminus,[39,40] we suggest that the folding routes for this L125A variant are similar to that of the WT and reference protein, although slightly more complex, with a primarily ground-state origin of the observed kinetic complexity. The data presented here and our previous equilibrium high-pressure results suggest that the energetic hierarchy of these variants remains similar to that of the true WT SNase, with the foldon architecture described by Bédard and co-workers,[46] and as in the case of apocytochrome $b_{562}$, unfolding by pressure and denaturant follows the same mechanism.[47]

In contrast to the reference protein and the L125A variant, the I92A variant, with the alanine substitution at the core of the most stable foldon, populates multiple ground-state intermediates involving disruption in all subdomains.[40] For this variant, the energetic hierarchy of states is completely scrambled, and conformers with much higher free energies relative to the states populated along the normal pathway in the WT and Δ+PHS variant become equally probable because the states in the normal hierarchy are strongly destabilized by the mutation. In addition to ground-state complexity, the site-specific structural information afforded by the pressure-jump NMR provides strong evidence for multiple folding routes and hence complexity at the folding barrier itself. Indeed, it is difficult to imagine that a folding/unfolding intermediate bearing a structured SubD1 and unstructured SubD2 could have folded via a TSE with an unstructured SubD1 and a structured SubD2. Likewise, an intermediate bearing an unstructured SubD1 and a structured SubD2 and IntD is unlikely to have folded via a TSE in which SubD1 was structured. While the schematics in Figure 6C are an oversimplification of the situation, they reinforce the notion that, structurally, these folding routes are mutually exclusive, and that unlike the simple hierarchy in the folding of the WT and reference proteins, a single alanine substitution deep in the protein's core leads to considerable complexification of the landscape. In addition to the structural arguments, the volumetric Hammond behavior of the TSE (note that void volume and surface area are not correlated[37]) and the denaturant dependence of the structural patterns of kinetic heterogeneity also support the conclusion that folding proceeds via multiple routes for this variant, which presents a highly heterogeneous ensemble at the barrier, as well (Figure 6). Moreover, for this variant, denaturant is likely to modulate the landscape at the barriers, as well as the relative fluxes through these distinct folding routes.

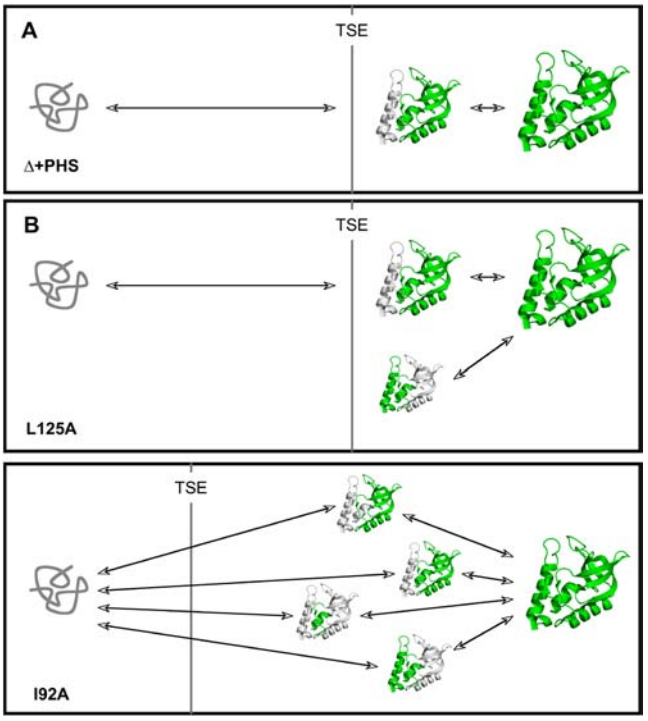


**Figure 6.** Schematic representation of the folding pathways of Δ+PHS, L125A, and I92A. Green color denotes the regions that are ordered. The line represents the position of the folding barrier along the reaction coordinate, which schematically is represented by number of native contacts, native contacts being in green. (A) Folding pathway of Δ+PHS, which is characterized by the presence of an intermediate state on the folded side of the main barrier,[30] and a native-like TSE with a disordered SubD2 and native-like SubD1. (B) Main folding barrier of L125A is similar to that of Δ+PHS; that is, native-like with a disordered SubD2 and native-like SubD1, but the free-energy landscape of this variant is populated by an additional intermediate state, with some degree of disorder in SubD1.[40] (C–E) Free-energy landscape of I92A presents a large conformational heterogeneity in the folded basin.[40] The folding barrier is quite early and the TSE structurally complex, representing multiple parallel folding routes.

## CONCLUSIONS

Owing to volume changes experienced by SNase during folding, the combination of pressure-jump relaxation and real-time multidimensional NMR spectroscopy has provided


dx.doi.org/10.1021/ja406682e | J. Am. Chem. Soc. 2013, 135, 14610–14618

unprecedented insight into the structural and energetic features of the folding reaction and of the transition-state ensemble. Chemical denaturant, which modulates the relative stabilities of the conformations both in the ground-state and at the folding barrier, further informed on the pathways for folding and underlying structural mechanisms.

One of the most important open issues in the protein folding field is whether proteins fold along a linear pathway by accretion of structure or whether they fold via parallel pathways. The present P-jump NMR kinetic measurements with a large number of observables probing distinct regions of the chain provide detailed structural information on folding mechanisms and pathways. Beyond its usefulness due to the slowing of folding rates and the multiple observables, pressure perturbation coupled to 2D NMR is uniquely useful to examine the kinetics of protein folding because pressure acts mainly by elimination of solvent-excluding voids, whose distribution throughout the protein is heterogeneous, unlike surface area, which is homogeneously distributed. Certain regions of proteins can be more poorly packed than others, and hence their stability is highly pressure sensitive, whereas other more tightly packed regions resist denaturation by pressure. The degree of cooperativity observed in pressure-induced unfolding in such cases will depend upon the energetic/structural coupling between the different domains. For these reasons, the study of pressure dependence of folding kinetics by 2D NMR facilitates the identification and characterization of the multiple conformations on a folding landscape and provides crucial information for understanding the sequence and structural determinants of this complex process. Because the structural basis for the effects of denaturants are homogeneously distributed throughout the protein, whereas those for pressure effects are not, denaturant and pressure do not always lead to the population of the same states during unfolding, and in general, denaturant will smooth the landscape compared to pressure.

Recently, quench flow, mass spectrometry, and H/D exchange have been used to demonstrate that RNase H1 folds via a linear pathway with stepwise accretion of structure.[48] Here we show that the wild-type SNase and the hyperstable Δ+PHS variant appear to fold via a linear pathway, as well, with a unique TSE in which the central cavity has been formed and in which the C-terminal SubD2 remains disordered. In the single intermediate basin on the folded side of the barrier, the C-terminus remains disordered, while the core is native-like. Introduction of a cavity at the interface between the two subdomains in SNase had negligible effects on this folding pathway; the TSE and the intermediate were very similar. Disorder in the N-terminus observed at equilibrium for the L125A variant[40] is likely to reflect off-pathway excited states. In contrast to this simple picture for the interfacial cavity, a cavity-creating substitution in the central core, I92A, with equivalent effects on the overall stability as the L125A substitution, led to multiple folding pathways and a structurally heterogeneous ensemble at the folding barrier exhibiting a low molar volume relative to the folded state. Higher complexity for early transition states has been predicted based on statistical arguments.[49,50] Thus, while the natural SNase and some variants thereof fold in a linear ordered fashion, this work, thanks to the site-specific nature of the kinetic measurements, shows that this need not be the case, and that a highly stable protein can exhibit very complex folding behavior, with multiple parallel folding pathways.

## MATERIALS AND METHODS

**Protein Engineering.** All experimental studies were performed on the wild-type SNase, the highly stable Δ+PHS variant,[51] and single-site variants of Δ+PHS. All proteins were engineered and purified as described previously.[39,51]

**Fluorescence-Detected P-Jump Kinetics.** Protein samples (50 μM) of the WT, Δ+PHS, and ΔPHS variants of SNase were dissolved in 50 mM Tris buffer at pH 7. The temperature was maintained at 293 K. GuHCl was added to the Δ+PHS and to the cavity-containing variants to enable the observation of a complete unfolding transition within the 3000 bar limit of our instrumentation. The following concentrations of GuHCl were used: Δ+PHS (2 M), V74A (1.4 M), I92A (1 M), L36A (1.3 M), L25A (1.2 M), L38A (1.8 M), F34A (0.8 M), V66A (1.2 M), L130A (1.0 M), L125A (1.2 M). Fluorescence measurements were made using an ISS steady-state fluorometer (Champaign, IL),[39] with an excitation wavelength of 290 nm and an emission wavelength of 340 nm. Positive pressure jumps of 200 bar were performed over the unfolding transition, and the fluorescence signal was recorded for a maximum of 240 min with an acquisition time of 5 s. The pressure-jump relaxation profiles at each pressure were well-fitted with a single-exponential decay model (see Figure S1).

For a simple two-state reaction, the P-jump relaxation time $\tau$ is the inverse sum of the folding ($k_f$) and unfolding rates ($k_u$):

$$\tau_{(p)} = \frac{1}{k_{f(p)} + k_{u(p)}} \quad (1)$$

The folding and unfolding rate constants are exponentially dependent on the pressure through the activation volume for folding reaction ($\Delta V_f^{\ddagger}$) and unfolding reaction ($\Delta V_u^{\ddagger}$), respectively:

$$k_{f(p)} = k_f e^{-p\Delta V_f^{\ddagger}/RT}$$

$$k_{u(p)} = k_u e^{-p\Delta V_u^{\ddagger}/RT} \quad (2)$$

The pressure dependence of the $\ln(\tau)$ was fitted using a nonlinear least-squares analysis to extract the values of the activation volume and folding/unfolding rates at atmospheric pressure. We constrained the $\ln(\tau)$ versus pressure fit using the recently published equilibrium volume change ($\Delta V_f^{o}$) and free-energy for folding ($\Delta G_f^{o}$) measured for the same proteins in the same conditions,[31] according to

$$\Delta G_f^{o} = -RT \ln\left(\frac{k_f}{k_u}\right) \quad (3)$$

and

$$\Delta V_f^{o} = \Delta V_f^{\ddagger} - \Delta V_u^{\ddagger} \quad (4)$$

**NMR-Detected P-Jump Kinetics.** Uniformly $^{15}$N-labeled samples of WT, Δ+PHS, and I92A, L125A, and V66A variants of Δ+PHS SNase were dissolved at 1 mM concentration in 300 μL 10 mM Tris buffer pH 7. $D_2O$ (10%) was added for the lock procedure. All NMR experiments were recorded at 293 K on a 600 MHz Bruker Avance III spectrometer equipped with a 5 mm Z-gradient $^1$H−X double-resonance broad-band inverse (BBI) probe. A commercial ceramic zirconia high-pressure NMR cell and an automatic pump system (Daedalus Innovations, Philadelphia, PA) were used to vary the pressure in the 1−2.5 kbar range. As for the fluorescence experiments, GuHCl was added to the Δ+PHS and Δ+PHS variant samples to decrease the protein stability so that pressures below 2.5 kbar were sufficient to observe a complete unfolding. For Δ+PHS and V66A that exhibit very long relaxation time, a series of $^{15}$N−$^1$H HSQC spectra,[52] with an acquisition time of 20 min, were recorded over 24 h after each positive 200 bar pressure jump. For I92A, L125A, and the WT SNase, a time series of $^{15}$N−$^1$H SOFAST HMQC[26−28] were recorded with acquisition time of 5 min (I92A) or 0.5 min (L125A and WT SNase). In all cases, the decay in the peak intensity of $^{15}$N−$^1$H amide cross-peaks was recorded after each positive 200 bar pressure jump. The jumps took less than 30 s, such that no dead time was apparent in the relaxation profiles. All NMR spectra were processed and analyzed


dx.doi.org/10.1021/ja406682e | J. Am. Chem. Soc. 2013, 135, 14610−14618

using GIFA.[53] The pressure dependence of the relaxation time $\tau$ measured for each amide group was individually fitted in a similar manner to the fluorescence experiments described above. For each residue, we independently constrained the $\ln(\tau)$ versus pressure fit using the recently published equilibrium data ($\Delta V_f^\circ$ and $\Delta G_u^\circ$),[40] measured for the same amide group, in the same condition.

## ■ ASSOCIATED CONTENT

### Supporting Information

Figure S1: P-jumps kinetics monitored by fluorescence. Figure S2: Pressure dependence of the relaxation time ($\tau$) measured from fluorescence P-jump experiments. Figure S3: Comparison of 2D $^{15}N-^{1}H$ HSQC spectra. Figure S4: P-jump kinetics monitored by NMR for WT SNase. Figure S5: Single-exponential fits of experimental HSQC peak intensity vs time profiles for all of the measured HMQC peak intensities for the reference protein and the I92A and L125A variants. Figures S6–S8: Distributions of the natural logarithm of the site-specific relaxation time ($\tau$) for Δ+PHS (Figure S5), L125A (Figure S6), and I92A (Figure S7). Figure S9: Site-specific $\Delta V_f^\circ$ and $\Delta V_f^\ddagger$ values presented as a function of the protein sequence for the reference protein, the L125A and the I92A variants. Figure S10: Comparison of the profiles of $\ln(\tau)$ vs pressure measured for I92A by fluorescence and by NMR. Figure S11: Structural heterogeneity of the $V_{TSE}$ for the I92A variant. Figures S12–S14: Heterogeneity in the site-specific $\ln(\tau)$ values collected for Δ+PHS (Figure S12), L125A (Figure S13), and I92A (Figure S14). This material is available free of charge via the Internet at http://pubs.acs.org.

## ■ AUTHOR INFORMATION


### Corresponding Author

catherine.royer@cbs.cnrs.fr

### Present Address

[#]Department of Biology and Center for Ciotechnology and Interdisciplinary Studies, Rensselaer Polytechnic Institute, Troy, New York 12180, United States

### Author Contributions

[‖]These authors contributed equally to this work.


### Notes

The authors declare no competing financial interest.

## ■ ACKNOWLEDGMENTS

We gratefully acknowledge support from the Agence National de la Recherche Grant PiriBio 09-455024 (CAR), Grants MCB-0743422 (BGME), MCB-0543769, and MCB-1050966 (AEG) from the National Science Foundation. D.R.N. was supported by a fellowship from Coordination for the Training and Improvement of Higher Education Personnel (CAPES) of Brazil, and J.R. was supported by a fellowship from the French Ministry of Research and Higher Education and a Fulbright International Graduate Fellowship.

## ■ REFERENCES


(1) Schuler, B.; Eaton, W. A. *Curr. Opin. Struct. Biol.* **2008**, *18*, 16–26.
(2) Nagarajan, S.; Taskent-Sezgin, H.; Parul, D.; Carrico, I.; Raleigh, D. P.; Dyer, R. B. *J. Am. Chem. Soc.* **2011**, *133*, 20335–20340.
(3) Killick, T. R.; Freund, S. M.; Fersht, A. R. *Protein Sci.* **1999**, *8*, 1286–1291.
(4) Balbach, J.; Steegborn, C.; Schindler, T.; Schmid, F. X. *J. Mol. Biol.* **1999**, *285*, 829–842.
(5) Steegborn, C.; Schneider-Hassloff, H.; Zeeb, M.; Balbach, J. *Biochemistry* **2000**, *39*, 7910–7919.
(6) Balbach, J.; Forge, V.; Lau, W. S.; van Nuland, N. A.; Brew, K.; Dobson, C. M. *Science* **1996**, *274*, 1161–1163.
(7) Limura, S.; Yagi, H.; Ogasahara, K.; Akutsu, H.; Noda, Y.; Segawa, S.; Yutani, K. *Biochemistry* **2004**, *43*, 11906–11915.
(8) Schanda, P.; Forge, V.; Brutscher, B. *Proc. Natl. Acad. Sci. U.S.A.* **2007**, *104*, 11257–11262.
(9) Li, H.; Frieden, C. *Proc. Natl. Acad. Sci. U.S.A.* **2007**, *104*, 11993–11998.
(10) Rennella, E.; Cutuil, T.; Schanda, P.; Ayala, I.; Forge, V.; Brutscher, B. *J. Am. Chem. Soc.* **2012**, *134*, 8066–8069.
(11) Udgaonkar, J. B.; Baldwin, R. L. *Nature* **1988**, *335*, 694–699.
(12) Roder, H.; Elove, G. A.; Englander, S. W. *Nature* **1988**, *335*, 700–704.
(13) Neudecker, P.; Lundstrom, P.; Kay, L. E. *Biophys. J.* **2009**, *96*, 2045–2054.
(14) Meinhold, D.; Wright, P. E. *Proc. Natl. Acad. Sci. U.S.A.* **2011**, *108*, 9078–9083.
(15) Akasaka, K.; Naito, A.; Nakatani, H. *J. Biomol. NMR* **1991**, *1*, 65–70.
(16) Akasaka, K.; Naito, T.; Imanari, M. *J. Am. Chem. Soc.* **1991**, *113*, 4688–4689.
(17) Akasaka, K.; Kawakami, M. In *Structure, Dynamics and Function of Biological Macromolecules*; Jardetsky, O., Finucane, M. D., Eds.; IOS Press: Amsterdam, 2001; pp 77–92.
(18) Kiefhaber, T.; Labhardt, A. M.; Baldwin, R. L. *Nature* **1995**, *375*, 513–515.
(19) Balbach, J.; Forge, V.; van Nuland, N. A.; Winder, S. L.; Hore, P. J.; Dobson, C. M. *Nat. Struct. Biol.* **1995**, *2*, 865–870.
(20) Hoeltzli, S. D.; Frieden, C. *Biochemistry* **1996**, *35*, 16843–16851.
(21) Guijarro, J. I.; Sunde, M.; Jones, J. A.; Campbell, I. D.; Dobson, C. M. *Proc. Natl Acad. Sci. U.S.A.* **1998**, *95*, 4224–4228.
(22) Killick, T. R.; Freund, S. M.; Fersht, A. R. *FEBS Lett.* **1998**, *423*, 110–112.
(23) Hoeltzli, S. D.; Frieden, C. *Biochemistry* **1998**, *37*, 387–398.
(24) Dobson, C. M.; Hore, P. J. *Nat. Struct. Biol.* **1998**, *5*, 504–507.
(25) Hoeltzli, S. D.; Frieden, C. *Proc. Natl Acad. Sci. U.S.A.* **1995**, *92*, 9318–9322.
(26) Schanda, P.; Kupce, E.; Brutscher, B. *J. Biomol. NMR* **2005**, *33*, 199–211.
(27) Gal, M.; Kern, T.; Schanda, P.; Frydman, L.; Brutscher, B. *J. Biomol. NMR* **2009**, *43*, 1–10.
(28) Gal, M.; Schandaa, P.; Brutscher, B.; Frydman, L. *J. Am. Chem. Soc.* **2007**, *129*, 1372–1377.
(29) Vidugiris, G. J.; Markley, J. L.; Royer, C. A. *Biochemistry* **1995**, *34*, 4909–4912.
(30) Brun, L.; Isom, D. G.; Velu, P.; Garcia-Moreno, B. E.; Royer, C. A. *Biochemistry* **2006**, *45*, 3473–3480.
(31) Mitra, L.; Hata, K.; Kono, R.; Maeno, A.; Isom, D.; Rouget, J. B.; Winter, R.; Akasaka, K.; Garcia-Moreno, B. E.; Royer, C. A. *J. Am. Chem. Soc.* **2007**, *129*, 14108–14109.
(32) Mohano-Borges, R.; Silva, J. L.; Ruiz-Sanchez, J.; de Prat-Gay, G. *Proc. Natl. Acad. Sci. U.S.A.* **1999**, *96*, 7888–7893.
(33) Pappenberger, G.; Saudan, C.; Becker, M.; Merbach, A. E.; Kiefhaber, T. *Proc. Natl. Acad. Sci. U.S.A.* **2000**, *97*, 17–22.
(34) Desai, G.; Panick, G.; Zein, M.; Winter, R.; Royer, C. A. *J. Mol. Biol.* **1999**, *288*, 461–475.
(35) Rouget, J. B.; Schroer, M. A.; Jeworrek, C.; Puhse, M.; Saldana, J. L.; Bessin, Y.; Tolan, M.; Barrick, D.; Winter, R.; Royer, C. A. *Biophys. J.* **2010**, *98*, 2712–2721.
(36) Royer, C. A. *Arch. Biochem. Biophys.* **2008**, *469*, 34–35.
(37) Rouget, J. B.; Akset, T.; Roche, J.; Saldana, J. L.; Garcia, A. E.; Barrick, D.; Royer, C. A. *J. Am. Chem. Soc.* **2011**, *133*, 6020–6027.
(38) Royer, C. A. *Biochim. Biophys. Acta* **2002**, *1595*, 201–209.
(39) Roche, J.; Caro, J. A.; Norberto, D. R.; Barthe, P.; Roumestand, C.; Schlessman, J. L.; Garcia, A. E.; Garcia-Moreno, B. E.; Royer, C. A. *Proc. Natl. Acad. Sci. U.S.A.* **2012**, *109*, 6945–6950.

(40) Roche, J.; Dellarole, M.; Caro, J. A.; Guca, E.; Norberto, D. R.; Yang, Y.; Garcia, A. E.; Roumestand, C.; Garcia-Moreno, B. E.; Royer, C. A. *Biochemistry* **2012**, *51*, 9536−9546.
(41) Vidugiris, G. S.; Truckses, D. M.; Markley, J. L.; Royer, C. A. *Biochemistry* **1996**, *35*, 3857−3864.
(42) Roche, J.; Caro, J. A.; Dellarole, M.; Guca, E.; Royer, C. A.; Garcia-Moreno, E. B.; Garcia, A. E.; Roumestand, C. *Proteins* **2013**, *81*, 1069−1080.
(43) Matouschek, A.; Fersht, A. R. *Proc. Natl. Acad. Sci. U.S.A.* **1993**, *90*, 7814−7818.
(44) Maki, K.; Cheng, H.; Dolgikh, D. A.; Shastry, M. C. R.; Roder, H. *J. Mol. Biol.* **2009**, *338*, 383−400.
(45) Maki, K.; Cheng, H.; Dolgikh, D. A.; Roder, H. *J. Mol. Biol.* **2007**, *368*, 244−255.
(46) Bédard, S.; Mayne, L. C.; Peterson, R. W.; Wand, A. J.; Englander, S. W. *J. Mol. Biol.* **2008**, *346*, 1142−1154.
(47) Fuentes, E. J.; Wand, J. A. *Biochemistry* **1998**, *37*, 9877−9883.
(48) Hu, W.; Walters, B. T.; Kan, Z. Y.; Mayne, L.; Rosen, L. E.; Marqusee, S.; Englander, S. W. *Proc. Natl. Acad. Sci. U.S.A.* **2013**, *110*, 7684−7689.
(49) Klimov, D. K.; Thirumalai, D. *J. Mol. Biol.* **1998**, *282*, 471−492.
(50) Chen, J.; Bryngelson, J. D.; Thirumalai, D. *J. Phys. Chem. B* **2008**, *112*, 16115−16120.
(51) Castaneda, C. A.; Fitch, C. A.; Majumbar, A.; Khangulov, V.; Schlessman, J. L.; Garcia-Moreno, B. E. *Proteins* **2009**, *77*, 570−588.
(52) Bodenhausen, G.; Ruben, D. J. *Chem. Phys. Lett.* **1980**, *69*, 185−189.
(53) Pons, J. L.; Malliavin, T. E.; Delsuc, M. A. *J Biomol. NMR* **1996**, *8*, 445−452.
(54) Till, M. S.; Ullmann, G. M. *J. Mol. Model.* **2010**, *16*, 419−429.